nature communications

Article

https://doi.org/10.1038/s41467-024-53755-8

Xeroderma pigmentosum protein XPD controls caspase-mediated stress responses

Received: 15 May 2024

Accepted: 22 October 2024

Published online: 29 October 2024

Check for updates

Hai Wei, Yi M. Weaver & Benjamin P. Weaver

Caspases regulate and execute a spectrum of functions including cell deaths, non-apoptotic developmental functions, and stress responses. Despite these disparate roles, the same core cell-death machinery is required to enzymatically activate caspase proteolytic activities. Thus, it remains enigmatic how distinct caspase functions are differentially regulated. In this study, we show that Xeroderma pigmentosum protein XPD has a conserved function in activating the expression of stress-responsive caspases in *C. elegans* and human cells without triggering cell death. Using *C. elegans*, we show XPD-1-dependent activation of CED-3 caspase promotes survival upon genotoxic UV irradiation and inversely suppresses responses to non-genotoxic insults such as ER and osmotic stressors. Unlike the TFDP ortholog DPL-1 which is required for developmental apoptosis in *C. elegans*, XPD-1 only activates stress-responsive functions of caspase. This tradeoff balancing responses to genotoxic and non-genotoxic stress may explain the seemingly contradictory nature of caspase-mediated stress resilience versus sensitivity under different stressors.

Caspases are cysteine proteases conserved across metazoans and best understood for their roles in cell death[1–3]. Non-lethal roles in cellular differentiation have also been identified for these same cell death caspases. In *Drosophila*, activation of caspase by a ubiquitin ligase is required for sperm development[4]. Across animal phyla, caspases have been shown to limit stemness. As examples, in mammals, caspase 3 targets Pax7 for muscle development[5] as well as Nanog to allow embryonic stem cell differentiation[6]. Additionally, in *C. elegans*, CED-3 caspase targets LIN-28 pluripotency factor in ectodermal stem cells to limit symmetric expansion of the stem pool[7] and promotes the asymmetric cell fate decision prior to cell death[8]. Caspases exhibit an array of functions during non-apoptotic neuronal development such as neuronal regeneration[9], control of arborization[10], formation of auditory circuitry[11] and axonal pruning[12].

In addition to developmental functions, these same caspases have emerging roles in regulating stress responses. The extent of responsiveness to diverse stressors was shown to be controlled by CED-3 caspase in *C. elegans*[13]. We further showed that CED-3 caspase limits a stress-priming function of a pathogen program to promote development[14] and this regulation controls neuronal integrity during aging[15]. The caspase-2/9 ortholog Dronc was shown to negatively regulate JNK to limit neoplastic transformation in a *Drosophila* tumor model[16]. With pronounced stress, JNK can also activate caspase-mediated production of ROS in a positive feedback manner converting the caspase from tumor suppressor to tumor promoter[17]. Moreover, TRAIL receptor signaling to caspase 8 is critical to link activation of NF-κB-dependent inflammatory processes with ER-stress responses altogether serving as a stress-induced molecular pattern[18].

Beyond altering classic stress-response pathways, emerging evidence suggests that caspases also regulate proteostasis and metabolic processes. As examples, the extended caspase family including both caspases and metacaspases have been shown to have important cytoprotective roles in resolving toxic protein aggregates[19]. Neurotoxicity induced by microglia requires caspase-dependent activation of PKC signaling in neurogenerative processes[20]. Further, it was demonstrated that the CED-3 cell death pathway in response to lipid oxidative stress was modulated by dietary fatty acids and host fatty acid metabolism[21]. More recently, we showed that CED-3 caspase activates a non-fatty acid synthesis function of FASN to limit stress responses[22].

In marked contrast to stress-suppressing functions, stress sensitivity rather than resistance can occur if caspase activities are compromised under various contexts. Aside from its role in cell death, caspase 2 promotes metabolic homeostasis where loss of caspase 2

Department of Pharmacology, University of Texas Southwestern Medical Center, Dallas, TX, USA. e-mail: benjamin.weaver@utsouthwestern.edu

function results in metabolic dysregulation and altered mitochondrial function[23] along with compromised antioxidant defenses[24] both contributing to premature ageing in the Casp2$^{-/-}$ mice. Following DNA damage, caspase 2 can be activated by nucleolar-localized PIDDosome in an NPM1-dependent manner[25]. Additionally, caspase 2 was shown as a driver of non-alcoholic steatosis and hepatitis as an outcome of ER-stress-induced SREBP1/2 activation[26]. Whether promoting or limiting stress responses or ultimately stress-induced cell death, it is clear that caspase activities are somehow coupled to both developmental and cellular stress responses. Thus, a major paradox remains as to how caspases are differentially regulated to execute divergent functions in development and stress responses. Further enigmatic, it is not clear why loss of caspase activity generates stress resistance in some contexts and stress sensitivity in other contexts.

In this work, we demonstrate that the highly conserved xeroderma pigmentosum gene XPD is critical for induction of caspase expression in both *C. elegans* and human cells. We further show that XPD-1 is required for stress-responsive induction of *ced-3* caspase independent of developmental cell deaths. Using proteomics for factors binding a DNA element upstream of the core *ced-3* promoter, we reveal that XPD-1 binds a probe generated from this DNA region. Tandem RNAi screens show the functional requirement for XPD-1 in limiting non-genotoxic stress responses. In contrast, we also show that compromising the *ced-3* promoter element, CED-3 caspase, or XPD-1 function leads to UV stress sensitivity and death. These findings reveal a tradeoff for caspase in promoting survival given a genotoxic insult and suppressing responsiveness to non-genotoxic stressors. In summary, our findings demonstrate that XPD has a conserved function in activating expression of stress-responsive caspases.

Results

Differential caspase expression in cell deaths and stress

Factors distinguishing regulation of apoptotic from non-apoptotic caspase activities remain elusive and a major area of limited understanding. It is further unclear whether altered caspase expression patterns are related to distinct activities. To address this, we examined modENCODE data and revealed a region of DNA upstream of the core *ced-3* promoter sequence enriched for more than 2 dozen transcription factors (Supplementary Fig. 1a). This putative upstream transcription factor-rich sequence (uTFs) is about 1 kilobase long (Fig. 1a). We used CRISPR mutagenesis to delete this region (Methods). Deletion of this region compromised dynamic changes in *ced-3* mRNA expression levels during development (Fig. 1b, Supplementary Fig. 1b, c). In wild type animals, *ced-3* mRNA is highly expressed in mid-stage embryos when programmed cell death is essential for tissue patterning. Shortly after hatching, *ced-3* mRNA decreased more than 100-fold in wild-type L1 larvae. Deletion of uTFs region further reduced *ced-3* mRNA about 50% in late-stage embryo and more than 90% in L1 larvae after developmental apoptosis is completed. In general, reduction of *ced-3* mRNA is more pronounced with absence of uTFs in the post-embryonic portion of the life cycle.

Using the *ced−1(e1735)* mutation to visualize cell corpses resulting from cell deaths[14,27], we found that deletion of the uTFs promoter region in *ced-3(uTFsΔ)* mutants only showed 33% reduction in mid-embryonic developmental cell deaths (Fig. 1c, d). This effect progressed into 43% reduction in early larval cell deaths (Fig. 1e–f). However, deletion of the uTFs compromised 100% adult-stage nerve cord cell deaths (Fig. 1g–i). This titration of caspase cell death function suggested that the uTFs promoter region was not essential but rather modulatory for caspase-mediated programmed cell deaths in early development.

To identify the functional impact of uTFs on *ced-3* functions, we analyzed phenotypes compared to the reference allele *ced-3(n717)*[28], hereafter *ced-3(-)*. Previously, we and others have reported that *ced-3(-)* null mutants have heightened responses to diverse stressors throughout larval development and into adulthood. In contrast to stage-specific defects in cell death, the *ced-3(uTFsΔ)* mutants with the uTFs promoter region deleted exactly phenocopied the *ced-3(-)* null mutants for heightened responsiveness in both early larval as well as adult stages to ER stress (Fig. 2a–c) and osmotic stress (Fig. 2d–f). In fact, the enhanced responses were seen in every developmental stage for both ER and osmotic stresses (Supplementary Fig. 2a–d). Thus, while modulatory for cell deaths, the uTFs region was essential for controlling the extent of *ced-3* stress responsiveness.

uTFs promoter region in stress-responsive caspase expression

The requirement for the uTFs region at every stage in stress responses but not cell deaths suggested the possibility of stress-induced expression of CED-3 caspase apart from developmental programmed cell death. To examine the impact of uTFs on spatiotemporal expression, we constructed a *ced-3* promoter reporter with and without the uTFs region (Fig. 3a). Using a histone-tagging approach[29], this reporter fused HIS-24 with mCherry to generate a punctate signal in the nucleus for ease of quantitation. To prevent perdurance of expression, we limited expression of the reporter prior to each experiment by using the auxin-induced degron (AID) tag (Supplementary Fig. 3a).

To limit autofluorescence from the body, we focused imaging and quantitation on the head region (Supplementary Fig. 3b). Consistent with *ced-3* caspase mRNA levels, the mCherry expression from the *ced-3* reporter transgene was more pronounced with intact uTFs sequence compared to the reporter without the uTFs sequence across all larval stages (Fig. 3b, c, Supplementary Fig. 3c–h) and adults (Fig. 3d–e). This enhanced expression with intact uTFs sequence was confirmed with Western analysis during embryonic development (Supplementary Fig. 3i), early larval development (Fig. 3f), and adulthood (Fig. 3g).

To determine the impact of stress on *ced-3* expression, we tested the *ced-3* reporter with and without the uTFs as a function of stress. We found that the both ER and osmotic stress induce *ced-3* reporter expression (Fig. 3h, Supplementary Fig. 3j–k). Because very little expression was observed in the absence of uTFs in adults (Fig. 3g–h), we tested *ced-3* reporter without the uTFs using L3 larvae. With over-exposure conditions of Western blot, we found the stress-induced expression was absent without the uTFs sequence (Fig. 3i). Thus, we concluded that uTFs sequence was necessary for induction of the *ced-3* reporter in both ER and osmotic stresses.

ced-3 promoter-binding proteins in stress responses

To identify proteins binding the uTFs region, we generated biotinylated DNA probes coupled to streptavidin beads and performed pull down with *C. elegans* lysates with protein ID using mass-spectrometry (Fig. 4a). As a negative control, we used a similar length DNA sequence generated from mCherry to control for non-specific binding. We obtained a cohort of DNA-binding factors enriched at least 2-fold in the uTFs probe pull down compared to negative control (Fig. 4b, Supplementary Fig. 4a and Supplementary Data 1).

To reveal the functional significance of these candidates, we performed tandem RNAi screens for both ER and osmotic stresses quantifying different stress-responsive reporters (Supplementary Fig. 4b–e). We analyzed all of the factors enriched by the proteomic analysis with predicted DNA binding activities (Orange circles in Fig. 4b, Supplementary Fig. 4a) along with all of the predicted factors from modENCODE data (Supplementary Fig. 1a). A confirmation analysis revealed 6 high priority candidates acting like *ced-3(-)* and *ced-3(uTFsΔ)* mutants to limit both ER and osmotic stress responsiveness (Fig. 4c, d).

CED-3 caspase functions distinguished by DPL-1 and XPD-1

The stage-specific defects in cell deaths along with stage-independent heightened stress-induced responses suggested the possibility of

https://doi.org/10.1038/s41467-024-53755-8

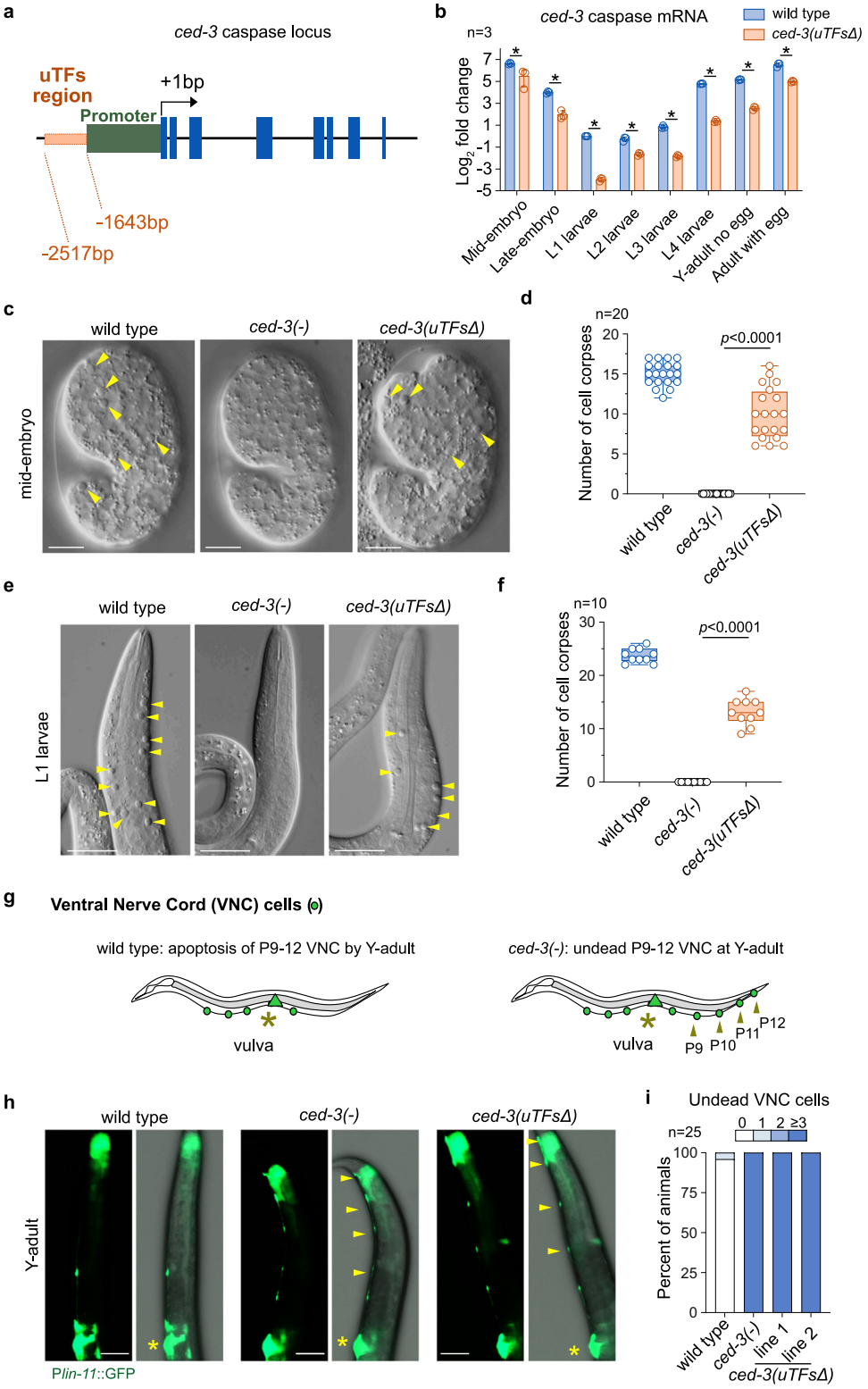

distinct functions mediated by factors binding to the uTFs sequence. When examining the impact of the 6 high priority candidates on *ced-3* mRNA levels, we found that *dpl-1* reduced *ced-3* expression the most in early larvae (Fig. 5a) whereas loss of *xpd-1* compromised adult expression of *ced-3* the most (Fig. 5b). Using the *ced-3* reporter, we confirmed the observation that loss of *dpl-1* had stronger effect on *ced-3* expression in early larvae (Fig. 5c, d) whereas *xpd-1* was important for adult-stage *ced-3* expression (Fig. 5e–f). To confirm the results for *xpd-1*, we used the *xpd-1(ve842)* allele which bears a large deletion of the coding sequence[30]. We found the *xpd-1(ve842)* allele also showed reduced expression of the *ced-3* reporter (Supplementary Fig. 5a).

Temporal examination of cell deaths showed that, regardless of the impact on *ced-3* level, *dpl-1* but not *xpd-1* was required in both early larval and adult-stage cell deaths (Fig. 5g–h). This finding is consistent with previous work demonstrating a critical role for DPL-1 in cell deaths by regulating the cell killing process[31]. Our temporal analysis for impact on stress response showed a different pattern where *dpl-1* was important in early larval stress responses (Fig. 5i–j, Supplementary

https://doi.org/10.1038/s41467-024-53755-8

Fig. 1 | Dynamic caspase gene expression during development requires *ced-3* upstream transcription factor site (uTFs). a Diagram of putative *ced-3* transcription factor-rich site (uTFs) upstream of core *ced-3* promoter. The *ced-3* core promoter (green) consists of −1 to −1643 bp from transcription start site. The uTFs region contains −1643 to −2517 bp (tan). The uTFs region was identified from modENCODE Chip-Seq data with multiple TFs binding this region. **b** The uTFs sequence is required for dynamic *ced-3* expression. qRT-PCR to measure expression of *ced-3* mRNA relative to *rpl-4* mRNA. Fold change compared to wild type L1 larvae plotted in $\log_2$ scale. *ced-3(uTFsΔ)* represents animals with deletion of uTFs in endogenous locus using CRISPR mutagenesis. Bar, mean value from three biological replicates. Error bar, SEM. See also Supplementary Fig. 1b-c for second set of primers. *, $p < 0.05$, two-tailed unpaired t-test. Individual p values of each stage provided in Source Data. Embryonic cell deaths modestly diminished in mutants lacking uTFs. DIC imaging (**c**) and quantitation (**d**) of mid-embryonic cell deaths. Yellow arrows indicate corpses of dying cells. The *ced-1(e1735)* mutation was used to visualize cell corpses[14,27]. Scale bar, 20 µm. Early larval cell deaths reduced less than 2-fold in mutants lacking uTFs. DIC imaging (**e**) and quantitation (**f**) of early L1 stage head corpses (yellow arrows). Scale bar, 20 µm. **d**, **f** Box extends from the 25th to 75th percentiles with the line in the middle plotted at the median. Whiskers plots minimum to maximum value. Each individual value as a point superimposed on the graph. n, number of animals. p value from two-tailed Mann−Whitney test. **g** Diagram of late larval cell deaths in ventral nerve cord (VNC) using the *Plin-11::GFP* transgene to visualize VNC lineage[31]. Yellow arrows indicate P9-12 undead VNC cells. Yellow star indicates position of vulva. Late larval cell deaths require uTFs region. DIC imaging (**h**) and quantitation (**i**) of early young adult stage VNCs retained in *ced-3(-)* and *ced-3(uTFsΔ)* mutants. Yellow arrows indicate P9-12 undead VNC cells. Yellow star indicates position of vulva. Scale bar, 50µm. Source data are provided as a Source Data file.

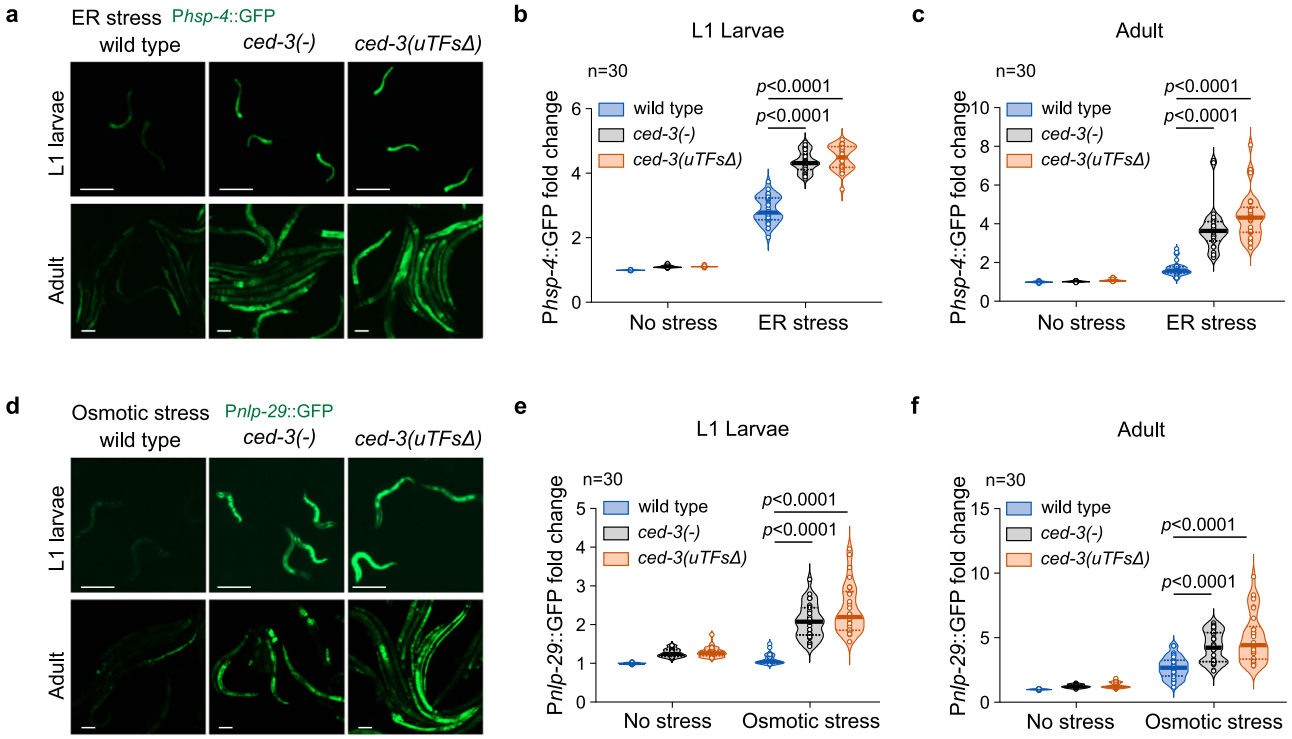

Fig. 2 | *ced-3*-dependent attenuation of stress response requires uTFs. a–**c** ER stress response heightened in *ced-3(-)* and *ced-3(uTFsΔ)* mutants. Fluorescence imaging of P*hsp-4::GFP* reporter (**a**) and quantitation of larval (**b**) and adult (**c**) animals with and without 6 µg/mL tunicamycin treatment. Scale bar, 100µm. Osmotic stress response heighted in *ced-3(-)* and *ced-3(uTFsΔ)* mutants. Fluorescence imaging of P*nlp-29::GFP* reporter (**d**) and quantitation of larval (**e**) and adult (**f**) animals with and without 400 mM NaCl treatment. Scale bar, 100µm. **b**, **c**, **e**, **f** center line, median value; n, number of animals; Fold change normalized to wild type no stress; p value from two-tailed Mann−Whitney test. Source data are provided as a Source Data file.

Fig. 5b) but not adult-stage stress responses (Fig. 5k–l, Supplementary Fig. 5c). In contrast, *xpd-1* was required for all stress responses including early larval (Fig. 5i–j, Supplementary Fig. 5b) and adult-stages (Fig. 5k–l Supplementary Fig. 5c). Therefore, we concluded that XPD-1 was a stress-specific regulator of *ced-3* caspase independent of developmental apoptosis.

To further understand the distinct roles of *xpd-1* and *dpl-1* in stress responses, we examined the impact of each on the induction of *ced-3* reporter under stress states. We find that XPD-1 is critical for adults to induce expression of the *ced-3* reporter in response to both ER stress (Fig. 5m) and osmotic stress (Fig. 5n). Under mock RNAi condition, *ced-3* reporter was readily induced in the presence of stressors. However, this induction was abolished with *xpd-1* RNAi (Fig. 5m–n). In contrast, DPL-1 was dispensable for this function in adults because the stress induced induction of *ced-3* reporter still persists with *dpl-1* RNAi (Fig. 5m–n). We also confirmed that animals treated with *xpd-1* RNAi abolished stress-responsive induction of endogenous CED-3 protein tagged with HA epitope (Supplementary Fig. 5d). Further, the *ced-3* reporter lacking the uTFs region failed to induce in response to ER or osmotic stress (Supplementary Fig. 5e–f). We observed higher basal levels of the *ced-3* reporter in the absence of stress under both *xpd-1* and *dpl-1* RNAi condition and found they were due to an elevated signal in the spermatheca (Supplementary Fig. 5g). These findings demonstrate distinct factors working to induce different functions of the same caspase (Fig. 5o).

XPD-1 and CED-3 caspase promote genotoxic stress survival

Because *xpd-1* was critical to induce non-apoptotic *ced-3* caspase expression, we considered whether human caspase expression required the human XPD ortholog (also known as XP-D or ERCC2).

https://doi.org/10.1038/s41467-024-53755-8

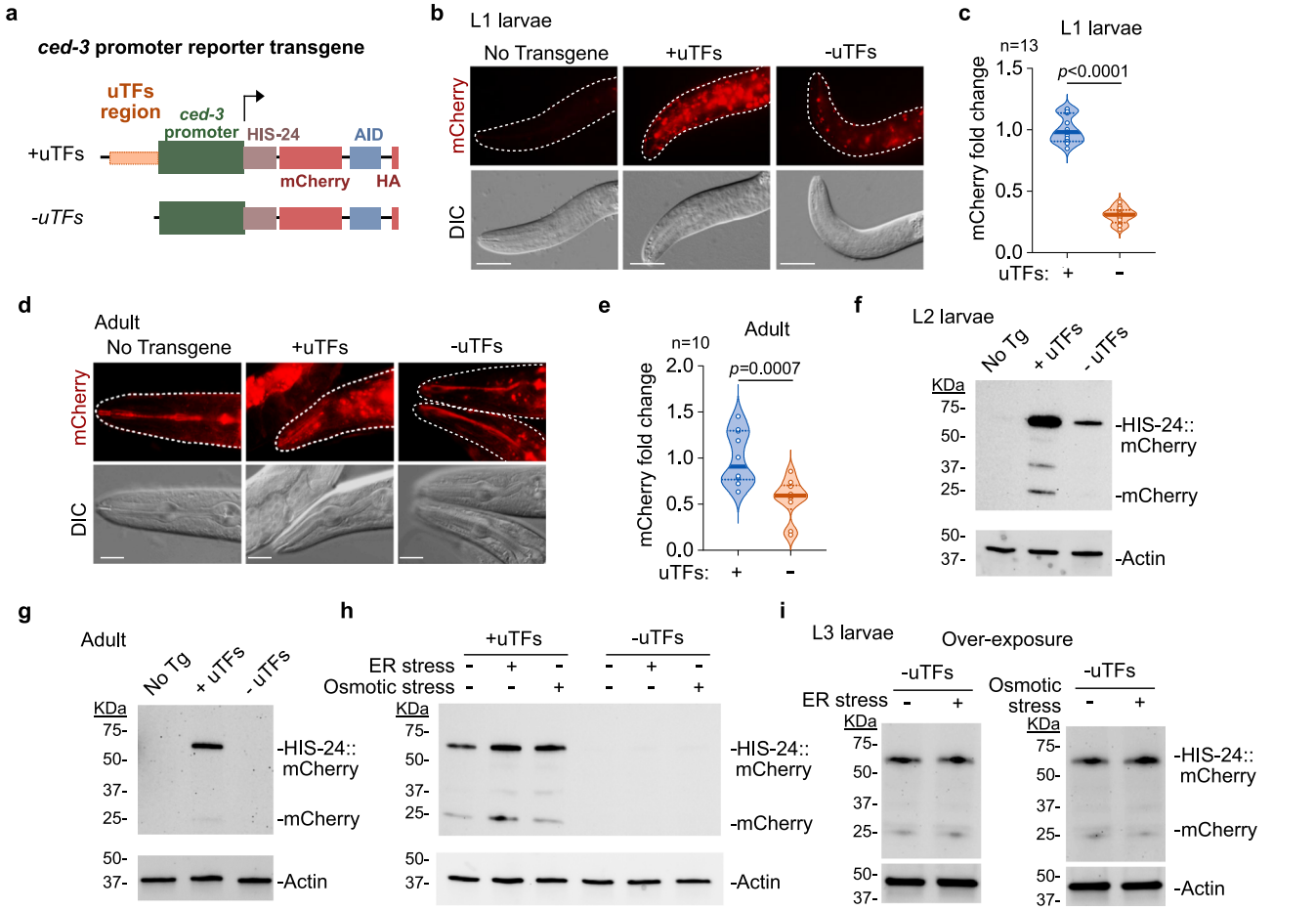

Fig. 3 | Developmental and stress-responsive induction of *ced-3* expression requires uTFs. a Diagram of *ced-3* reporter transgene cassettes with and without uTFs region. The *ced-3* core promoter (green) consists of −1 to −1643 bp from transcription start site. The uTFs region contains −1643 to −2517 bp (tan). Reporter generates a His-24::mCherry::HA fusion protein that was detected using anti-HA antibody. Expression of reporters was controlled by auxin induced degron (AID). Reporters were inserted into the same MosI site to control for ectopic location of reporter. Fluorescence imaging analysis shows early larval stage and young adult animals have compromised expression of *ced-3* reporter without uTFs region. Early larvae fluorescence and DIC imaging (**b**) and (**c**) quantitation. Young adult fluorescence and DIC imaging (**d**) and (**e**) quantitation. **b** Scale bar, 20 µm. **d** Scale bar, 50 µm. **c**, **e** center line, median value; p value from two-tailed Mann−Whitney test. Western analysis shows early larvae (**f**) and young adults (**g**) have compromised expression of *ced-3* reporter without the uTFs region. **h**, **i** Stress-responsive induction of *ced-3* reporter requires uTFs region with ER and osmotic stressors. **h** Adults show induction of *ced-3* reporter with ER and osmotic stresses with intact uTFs region. **i** Overexposed gels for mid-larval animals show no induction of *ced-3* reporter lacking uTFs region with ER or osmotic stress. **f**, **g**, **h**, **i** each experiment was repeated independently twice with similar results. HIS-24:mCherry reporter was detected using anti-HA antibody. Source data are provided as a Source Data file.

Examination of mRNA levels in HEK 293 cells by qRT-PCR showed that *xpd* siRNA efficiently knocked down endogenous *xpd* mRNA levels (Supplementary Fig. 6a). Upon knock-down of *xpd* levels, we find that caspases 1, 2, 7 and 9 mRNAs had reduced expression when treated with *xpd* siRNA (Fig. 6a). Moreover, not all caspases were altered in expression by *xpd* siRNA suggesting the possibility of XPD-specific caspase activation.

Consistent with the role of XPD in UV-induced DNA damage repair in patients with xeroderma pigmentosum (XP), we also found that *xpd* siRNA in HEK 293 cells results in enhanced sensitivity to UV irradiation (Supplementary Fig. 6b–c). In fact, cells treated with *xpd* siRNA showed no recovery following irradiation (Supplementary Fig. 6d). We set out to determine the functional significance of *ced-3* expression and XPD function in survival on genotoxic UV stress in *C. elegans*. We found that disruption of CED-3 function by either *ced-3(-)* or *ced-3(uTFsΔ)* mutation compromised adult survival following UV irradiation (Fig. 6b–c). There was no difference on adult survival over the same period in the absence of UV (Supplementary Fig. 6e). In addition, early larvae of *ced-3(-)* and *ced-3(uTFsΔ)* mutants also showed compromised survival with UV irradiation (Supplementary Fig. 6f). Consistent with this, treatment of animals with *xpd-1*(RNAi) compromised survival with UV irradiation for adults (Fig. 6d, Supplementary Fig. 6g) as well as early stage larvae (Fig. 6e, Supplementary Fig. 6h). Disruption of XPD-1 function in mutants with the *xpd-1(ve842)* allele also compromised survival with UV stress compared to animals without UV stress over the same period (Fig. 6f, Supplementary Fig. 6i). Loss of CED-3 catalytic activity with the *ced-3(n2433)* mutation[28] or loss of the upstream activating factor *ced-4 (Apaf)* with the *ced-4(n1162)* mutation similarly compromised survival for adults treated with UV stress (Fig. 6g) as well as early larvae (Supplementary Fig. 6j) compared to animals not treated with UV (Supplementary Fig. 6k).

XPD-1 and CED-3 caspase limit non-genotoxic stress survival

The compromised UV survival results are intriguing because under non-genotoxic stress conditions such as ER and osmotic stress, disruption of *ced-3* or *xpd-1* lead to heightened stress responses. Consistent with this observation, and in stark contrast to genotoxic UV irradiation, we found that both the *ced-3(−)* and *ced-3(uTFsΔ)* mutation enhance survival on ER stress (Fig. 6h) as well as osmotic stress (Supplementary Fig. 6l). Consistent with this, *xpd-1*(RNAi) also enhanced

https://doi.org/10.1038/s41467-024-53755-8

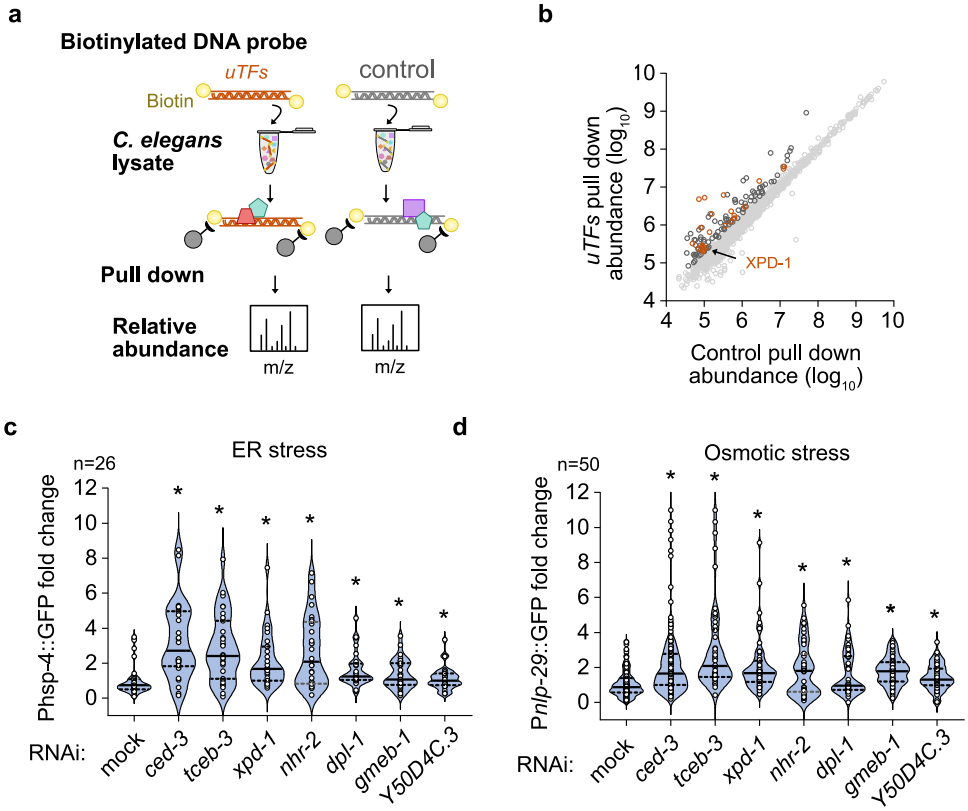

Fig. 4 | Proteomic identification and stress-responsive RNAi screen reveals factors binding uTFs. a Overview of proteomics approach using biotinylated DNA probes. Biotinylated uTFs and mCherry (control) probes were generated with PCR and bound to streptavidin beads. **b** Mass-spec reveals 136 factors (black circle) enriched in uTFs probe versus mCherry DNA (control) of which 26 contain DNA binding activity (orange). **c**, **d** Top candidates from functional RNAi screen of 58 factors revealed by proteomics (Supplementary Fig. 4a) and modEncode factors (Supplementary Fig. 1a) for altered ER and osmotic stress responsiveness. *, $p < 0.05$, two-tailed Mann–Whitney test. n, number of animals. Individual p values of each RNAi treatment provided in Source Data. Source data are provided as a Source Data file.

survival on ER stress (Fig. 6i) and osmotic stress (Supplementary Fig. 6m). As confirmation, we found that the *xpd-1(ve842)* mutation caused a notable developmental delay in the absence of stress (Supplementary Fig. 7a–b) yet those mutants exhibited more resistance to ER stress than wild type (Supplementary Fig. 7b) and showed significant compromise in survival with UV stress (Supplementary Fig. 7c).

In contrast to *C. elegans*, cells treated with *xpd* siRNA showed no net impact on HSP5A induction with ER stress (Supplementary Fig. 7d). However, knocking down *caspase-1* enhanced HSP5A mRNA levels whereas knock down of *caspase-2* diminished HSP5A mRNA levels in response to ER stress (Supplementary Fig. 7d). These findings suggest that although XPD controls expression of multiple caspases in mammals, the consequence of individual caspase activation may depend on tissue and cellular context.

XPD-1 promotes stress-responsive CED-3 expression

To test the possibility that expression of *ced-3* caspase regulated by XPD-1 is dependent on individual stressors, we tested induction of *ced-3* reporter under UV irradiation. We found that UV stress strongly induced the *ced-3* reporter (Fig. 6j). Importantly, induction of the *ced-3p*::mCherry reporter expression by UV irradiation required intact XPD-1 function where *xpd-1*(RNAi) treated animals failed to induce *ced-3* with UV (Fig. 6j). This pattern was confirmed for expression of CED-3 protein (Supplementary Fig. 7e). Moreover, the reporter lacking the uTFs region also failed to induce during UV stress (Supplementary Fig. 7f). In addition, loss of *gtf-2h1* (BTF2 p62) also failed to induce expression the mCherry reporter while other TFIIH factors did not show an obvious impact on induction (Supplementary Fig. 7g–h).

Because CED-3 catalytic activity was required, we sought to understand what substrates might be involved. We previously showed that PMK-1 and FASN-1 were proteolytic substrates of CED-3 in non-genotoxic stress responses including ER, osmotic, and ROS stresses[14,15,22]. We find that a double cleavage-resistant mutant *pmk-1(D327E); fasn-1(D1593E)* had severely compromised development with UV irradiation during early larval development comparable to *ced-3(-)* and *ced-3(uTFs)* mutants (Fig. 7a) but not during adulthood (Fig. 7b). The double mutant had no phenotype during the same period of adult in the absence of stress (Supplementary Fig. 7i). The individual mutants reveal that *fasn-1(D1593E)* had stronger impact than *pmk-1(D327E)* during early larval UV stress (Supplementary Fig. 7j) but *pmk-1(D327E)* had more impact, although not statistically significant, during adult UV stress (Supplementary Fig. 7k). Neither mutant had a negative impact without stress (Supplementary Fig. 7l).

Germline CED-3 contributes to organismal stress response

Given the function of *xpd-1* in germline DNA repair following UV damage[32], we next sought to understand the relative contributions of germline and somatic tissues. We find that ablated germline with the *glp-4(bn2)* allele at the non-permissive temperature led to less of a difference in survival disadvantage for *ced-3(RNAi)* and *xpd-1(RNAi)* compared to mock RNAi in larval development (Fig. 7c) and adult survival (Supplementary Fig. 8a). Conversely, removal of germline also resulted in reduced protection provided by *ced-3(RNAi)* or *xpd-1(RNAi)* with ER stress (Fig. 7d) and osmotic stress (Supplementary Fig. 8b). These findings suggest that cross-tissue communication is essential for organismal stress responses.

https://doi.org/10.1038/s41467-024-53755-8

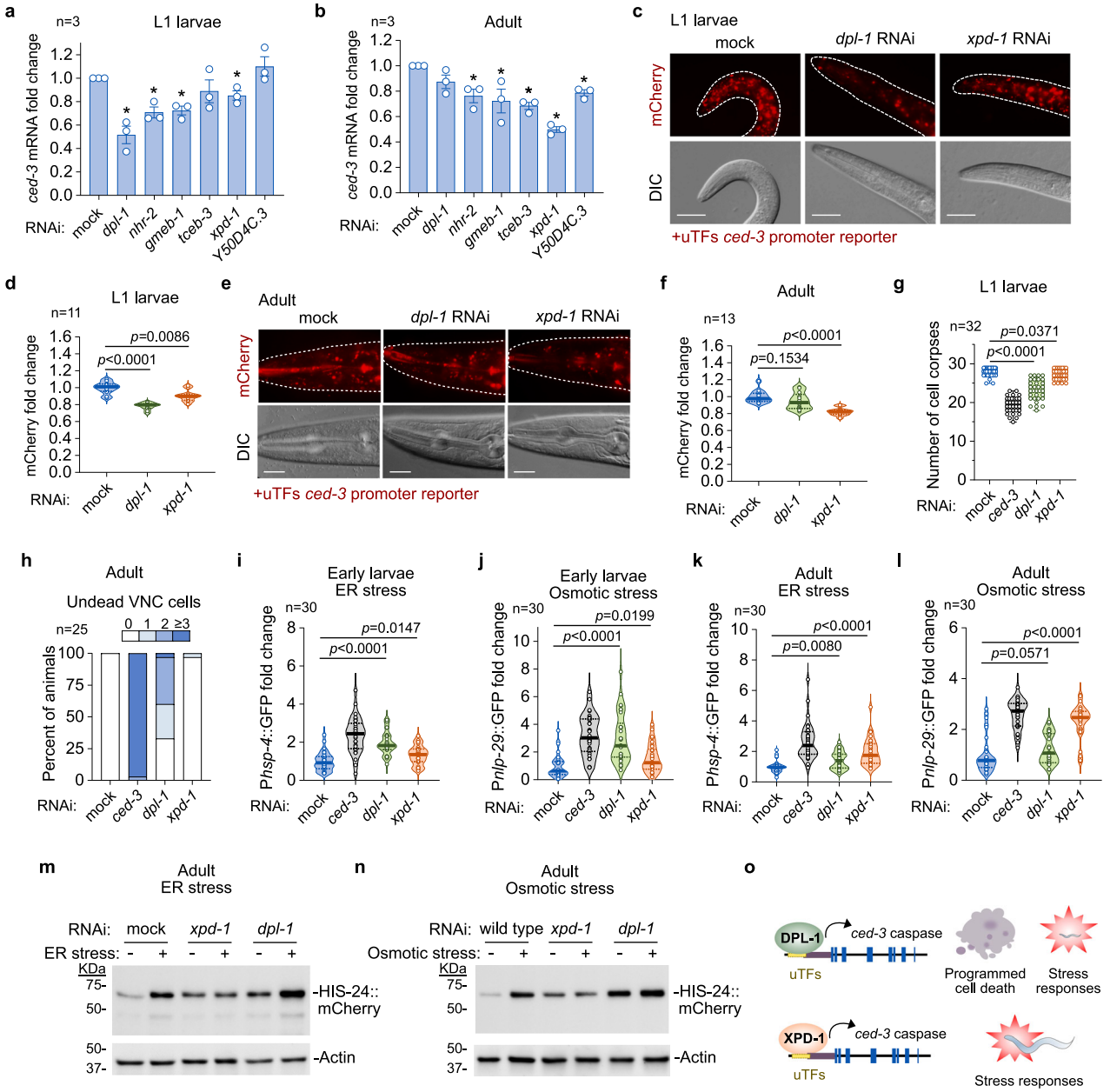

Fig. 5 | DPL-1 and XPD-1 differentially regulate CED-3 caspase function in cell death and attenuation of stress responses. a, **b** Impact on *ced-3* mRNA expression by *dpl-1* in early larvae and *xpd-1* in young adults. qRT-PCR to measure expression of *ced-3* mRNA relative to mock RNAi. Bar, mean value from 3 biological replicates. Error bar, SEM. *, $p < 0.05$, two-tailed unpaired t-test. Individual p values of each RNAi treatment provided in Source Data. Expression of *ced-3* reporter mostly regulated by DPL-1 in early larvae. Early larvae fluorescence and DIC imaging (**c**) and (**d**) quantitation. Scale bar, 20μm. **e**–**f** Expression of *ced-3* reporter regulated by XPD-1 in adults. Young adult fluorescence and DIC imaging (**e**) and (**f**) quantitation. Scale bar, 50 μm. **d**, **f** center line, median value; p value from two-tailed Mann–Whitney test. **g**–**h** DPL-1 but not XPD-1 required in both larval and adult cell deaths. **g** DPL-1 but not XPD-1 required in early larval cell deaths and (**h**) adult-stage ventral nerve cord cell deaths. **g** box extends from the 25th to 75th percentiles with the line in the middle plotted at the median. Whiskers plots minimum to maximum value. Each individual value as a point superimposed on the graph. p value from two-tailed Mann–Whitney test. **i**–**j** DPL-1 and XPD-1 required for early larval attenuation of ER stress responses tunicamycin (**i**) and osmotic stress with NaCl (**j**) in early larvae. XPD-1 but not DPL-1 required for attenuation of ER stress with tunicamycin (**k**) and osmotic stress with NaCl (**l**) in young adults. **i**, **j**, **k**, **l** center line, median value; p value from two-tailed Mann–Whitney test. XPD-1 required for stress-responsive induction of *ced-3* reporter under ER stress with tunicamycin (**m**) and osmotic stress with NaCl (**n**) in young adults. RNAi treatment started at L1 and stress treatment started at L4. Sample collection at young adult stage. HIS-24::mCherry reporter was detected using anti-HA antibody. **o** Diagram of DPL-1 and XPD-1 working on uTFs region to support distinct caspase functions. Source data are provided as a Source Data file.

We next tested for accumulation of DNA damage by monitoring accumulation of the photoproduct cyclobutane pyrimidine dimers (CDPs). Consistent with the UV-sensitive phenotype, disruption of *ced-3* function by *ced-3(-)* or *ced-3(uTFsΔ)* mutation led to enhanced accumulation of CDPs following UV irradiation (Supplementary Fig. 8c). Similarly, *ced-3(RNAi)* and *xpd-1(RNAi)* also enhanced CDP accumulation following UV stress (Supplementary Fig. 8d). However, the accumulation of DNA damage by treatment of *ced-3* or *xpd-1* RNAi was masked with germline ablation (Supplementary Fig. 8e). To further understand the distinct contributions of CED-3 in germline and somatic tissues, we generated a functional auxin-induced degron (AID)-tagged CED-3 allele (Supplementary Fig. 8f–h). Removal of whole

https://doi.org/10.1038/s41467-024-53755-8

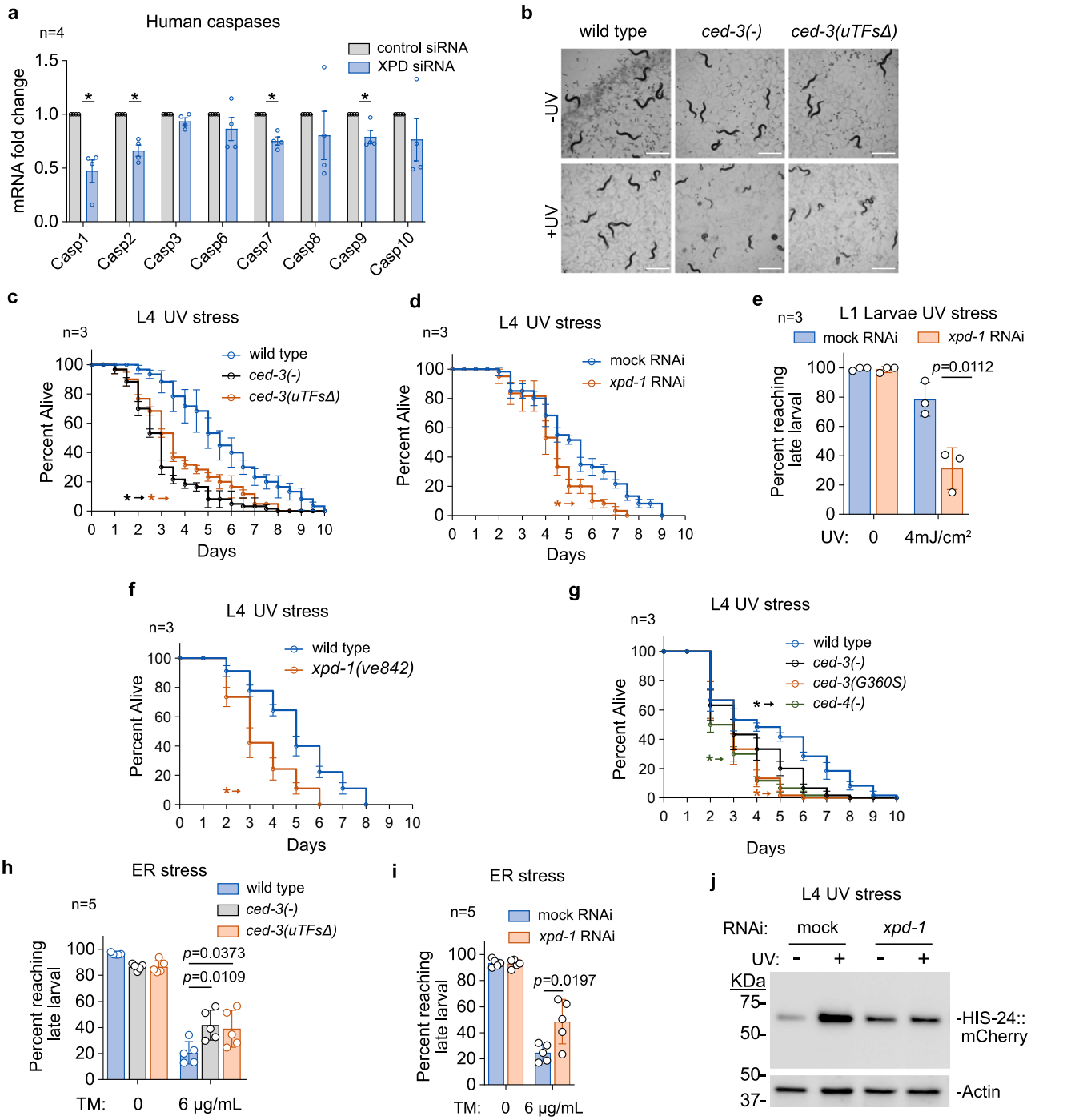

Fig. 6 | Conservation of XPD in caspase expression controls non-apoptotic stress responses. a Cohort of human caspases with expression supported by XPD factor. HEK cells treated with *xpd* siRNA reduces expression of several caspases as measured by qRT-PCR. Bar, mean value from 4 biological replicates. Fold change normalized to control siRNA for each individual caspase. Error bar, SEM. *, $p < 0.05$, two-tailed unpaired t-test. **b**–**c** Diminished survival in the *ced-3(-)* and *ced-3(uTFsΔ)* mutants with genotoxic stress. (**b**) Plate phenotype (-UV 0 h vs +UV 48 h) and (**c**) survival curve of mid-L4 animals treated with 75 mJ/cm² UV radiation. Scale bar, 250 µm. **d** Diminished survival with genotoxic stress in animals treated with *xpd-1* RNAi. Survival curve of mid-L4 animals treated with 100 mJ/cm² UV radiation. **e** Enhanced developmental delay in animals treated with *xpd-1* RNAi before exposing to 4mJ/cm2 UV at L1 larval stage. Bar, mean value from 3 biological replicates. Error bar, SD. p value from two-tailed unpaired t-test. **f** Diminished survival with genotoxic stress in *xpd-1(ve842)* mutants. Survival curve of early-L4 animals treated with 75 mJ/cm² UV radiation. **g** Diminished survival with genotoxic stress in strains with active site dead *ced-3(G360S)* or *ced-4(-)* mutation. Enhanced survival under ER stress with tunicamycin treatment in *ced-3(-)* and *ced-3(uTFsΔ)* mutants (**h**) and *xpd-1* RNAi (**i**). **h**, **i** bar, mean value from 5 biological replicates. Error bar, SD. p value from two-tailed unpaired t-test. **j** XPD-1 required for genotoxic stress-responsive induction of *ced-3* reporter. Western blot of *ced-3* promoter reporter of mid-L4 animals treated with and without UV radiation (75 mJ/cm²). HIS-24::mCherry reporter was detected using anti-HA antibody. **c**, **d**, **f**, **g** mean value from 3 biological replicates. Error bar, SD. Star with arrow marks the starting time in adulthood when $p < 0.05$ compared to wild type or mock RNAi. p value from two-tailed unpaired t-test. Individual p values provided in Source data. Source data are provided as a Source Data file.

https://doi.org/10.1038/s41467-024-53755-8

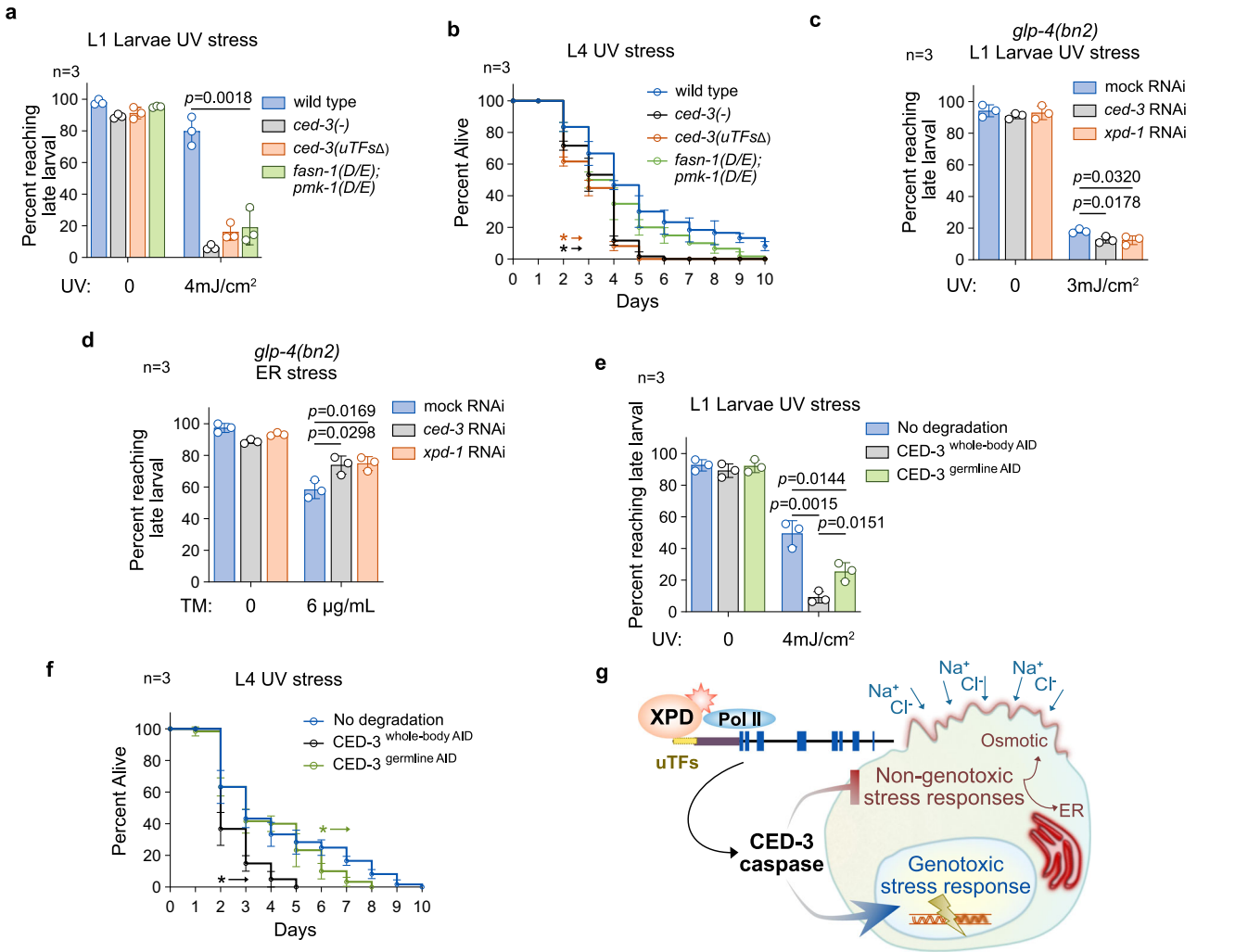

Fig. 7 | XPD-1 and CED-3 mediate stress responses with contributions from both germline and somatic tissues. a Developmental delay in caspase-cleavage resistant double mutant animals exposed to 4mJ/cm2 UV at L1 larval stage. **b** Survival with genotoxic stress in mutants with two caspase substrates with cleavage resistant mutations. **c**–**d** Diminished difference in *glp-4(bn2)* mutants without germline treated with *ced-3* and *xpd-1* RNAi compared to mock RNAi before exposing to 4mJ/cm^2 UV at L1 larval stage (**c**) or under ER stress with tunicamycin treatment (**d**). **e**–**f** Developmental delay of germline specific elimination of CED-3 before exposing to 4mJ/cm^2 UV at L1 larval stage (**e**) and survival curve of mid-L4 animals treated with 75 mJ/cm^2 UV radiation (**f**). **g** Diagram of XPD supporting expression of caspase for opposing functions in genotoxic versus non-genotoxic stress responses. **a**, **c**–**e** bar, mean value from 3 biological replicates. Error bar, SD. p value from two-tailed unpaired t-test. **b**, **f** mean value from 3 biological replicates. Error bar, SD. Star with arrow marks the starting time in adulthood when $p < 0.05$ compared to wild type or no degradation condition. Two-tailed unpaired t-test. Individual p values of each day in adulthood provided in Source data. Source data are provided as a Source Data file.

body CED-3 showed a strong compromise in development and adult survival with UV irradiation (Fig. 7e–f). Whereas, loss of germline CED-3 alone showed significant impact but less than whole body removal of CED-3 with UV irradiation (Fig. 7e–f). We observed similar pattern with ER stress (Supplementary Fig. 8i–j). Our results suggest that XPD-1 induces *ced-3* expression under all stress conditions tested regardless of the nature of the stressor with contributions of both germline and somatic tissues. In summary, our findings reveal that XPD-1 is critical for induction of CED-3 caspase expression independent of cell death function to promote genotoxic stress survival while blocking non-genotoxic responses (Fig. 7g).

Discussion

It has been a long-standing mystery why caspases have remained so highly conserved when many caspase mutants are viable and often show enhanced resistance to many stressors. The conservation of caspases across all animal phyla suggests a strong selection pressure. Our findings reveal a tradeoff for enhanced survival on non-genotoxic stressors in the absence of CED-3 caspase with a concomitant loss of survival in the face of genotoxic stressors. Intriguingly, rather than having distinct factors activating caspase under different stressors, we find that XPD activates these two divergent functions carried out by the same caspase: limiting responses to non-genotoxic stressors which threaten harm to a cell, while promoting genotoxic stress responses which threaten harm to the genome. Recent work has shown this threat can emerge in a transgenerational manner[33]. Intriguingly, genotoxic insults themselves display tradeoffs where evolution has selected for repair pathways leaving relatively small base substitution errors over large deletions[34].

We further show that requirement of XPD for expression of stress-responsive caspases is conserved from nematodes to human cells. XPD works in DNA damage repair, chromosome segregation[35] and is part of the basal transcriptional activation factor TFIIH providing DNA helicase activity with 5′ to 3′ polarity[36–38]. We find that one other TFIIH

factor, *gtf-2h1* (BTF2 p62) was also required for *ced-3* reporter induction but *gtf-2h4* (BTF2 p52) and the associated CDK-7 kinase were not. Numerous studies have worked to dissect the impact of distinct human *xpd* mutations to protein structure and function as well as understand the assembly and function of the TFIIH complex[35–41]. As the distinct *XP* complementation groups have distinct functions, it is further interesting that distinct DNA repair mechanisms are operative throughout the life history of an organism[42,43]. Further, it was previously shown that *gtf-2h5* (TTDA) which stabilizes the TFIIH complex in multiple tissues is not essential for survival except when challenged with DNA damage[44]. Given the three distinct clinical diseases resulting from different mutations in the *xpd* gene, this has led to speculation of possibly multiple diverse transcriptional functions for XPD that we do not currently understand[39,45].

In fact, XPD is conserved from archaea through all eukaryotes. Also, previous work revealed that XPD supports p53-mediated cell death and injection of caspase 1 or caspase 2 rescues apoptosis when *xpd* function is compromised in *xeroderma pigmentosum* patient cells with *xpd* mutations[41]. Recently it was shown that sub-lethal levels of stress that alter mitochondrial integrity can activate caspase within the cell leading to CAD-dependent DNA damage[46]. Moreover, loss of *xpd-1* function in germline can trigger cell deaths ultimately causing degeneration of the tissue[32]. With our findings that XPD-1 coordinates induction of caspase genotoxic and non-genotoxic responses in *C. elegans*, it is intriguing to consider how an XPD-caspase regulatory circuit might have arisen early in animal evolution. Further, because caspases 1, 2, 7 and 9 have all been shown to mediate inflammatory and stress responses in mammals[24,26,47–51] along with the current findings, it is intriguing to consider the possibility that the accumulation of caspase orthologs in the evolution of mammals allowed for diversification of functions. It remains unclear how XPD-1 and CED-3 mediate opposing responses to genotoxic and non-genotoxic responses. While we found that the proteolytic targets FASN-1 and PMK-1 were important for survival with UV irradiation during early larval development, they were not required at late larval development suggesting stage-dependent targets that we do not yet understand. Additionally, the opposing responses to genotoxic and non-genotoxic stresses may also depend on cellular milieu where stress-specific changes in cell signaling cascades, gene expression or metabolism alters accessibility of targets. As a further limitation to our findings, we did not assess the impact of the proteolytic targets FASN-1 or PMK-1 on accumulation of DNA damage. Thus, additional CED-3 targets could also be important for stress survival even at early larval stages to prevent accumulation of DNA damage.

Understanding differential regulation of caspase functions has been enigmatic. There is evidence for sub-cellular compartmentalization of caspase activity to provide a non-apoptotic compartment within a cell[52]. Adding to the complexity, cross-tissue signaling between germline and somatic tissues has been shown as important for supporting and priming stress responses which is important given somatic tissues have limited repair capacity compared to germline[53–58]. In this study, we find that germline does play an important role in stress responses and *xpd-1* along with *ced-3* appear to have stress-responsive functions in both germline and somatic tissues. Yet the factors distinguishing when caspase is expressed outside of cell death remain unclear. Our findings reveal that caspase expression can be induced by XPD in the absence of programmed cell deaths to promote cell survival under stress. It is intriguing that DPL-1 and XPD-1 with distinct spatiotemporal regulation of caspase functions related to death and stress response are also both highly conserved DNA damage response factors[31,38,45]. Future studies will be required to understand the spatiotemporal inputs coordinating non-lethal activation of caspases and how stress-responsiveness and developmental processes are integrated.

Methods

C. elegans culture

All strains were maintained at 20 °C well fed on OP50 before the experiments. For RNAi experiments, RNAi constructs were expressed in the HT115 bacteria and seeded on NGM plates supplemented with 200 µg/mL Ampicillin and 1 mM IPTG. See Supplementary Table 1 for strains used in the study. *glp-4* (*bn2*ts) mutant was maintained at 12 °C and synchronized L1 were then shifted to 25 °C for RNAi and stress treatments.

CRISPR mutagenesis

CRISPR mutagenesis was used to generate uTFs deletion mutation, *ced-3* promoter reporter and endogenously AID (auxin induced degron)-tagged CED-3. Specifically, *ced-3*(uTFsΔ) and CED-3::AID mutants were generated using short-range HDR with dpy-10 co-CRISPR method in the endogenous genomic locus. For *ced-3* promoter reporter strains, an single-copy transgene of *ced-3*p::His-24::mCherry::AID::HA, with or without uTFs sequence was inserted into the same Mos1 transposon site LGIII Mos1_ oxTi444 using the SEC CRISPR-Cas9 method. See Supplementary Table 2 for sgRNA sites.

Human cell culture and siRNA transfections

HEK293 cells (ATCC, CRL-1573) maintained in 10% FBS with high glucose DMEM, antibiotic and antimycotic. The siRNA transfections used Lipofectamine RNAiMAX (Invitrogen™ 13778075) and Control siRNA and *xpd* (ERCC2) siRNA (5nmol SMARTpool, Horizon Discovery Bioscience).

mRNA extraction and qRT-PCR for *ced-3* and human *Caspases*

mRNA of synchronized *C. elegans* at different stages was extracted using TRIzol reagent (Invitrogen, 15596-026). mRNA of HEK cells was extracted using Monarch Total RNA kit (NEB, T2010). For *C. elegans*, three independent biological replicates of each stage, treatment and genotype were collected for qRT-PCR analyses using BioRad CFX Maestro v1.1. For each biological sample, three technical replicates were analyzed. For HEK cells, three to four independent biological replicates of each treatment were collected and for each biological sample, three to four technical replicates were analyzed. See Supplementary Table 3 for oligos used for qRT-PCR.

Scoring cell deaths

Head corpses were analyzed using the *ced-1(e1735)* allele[14,27]. Ventral nerve cord cell deaths were analyzed using the P*lin-11::GFP* reporter[31]. For counting early L1 head corpses, bleached embryos in M9 were used to obtain L1 larvae just at hatching. Animals were then imaged on 2% agarose pads with a Zeiss Nomarski. For counting cell corpses of comma-stage embryonic development, embryos obtained from bleaching were washed and collected in M9. Comma-stage embryos were identified visually on 2% agarose pads with a Zeiss Nomarski microscope. Views from multiple focal planes and multiple positions were used to calculate the total number of cell corpses in a given sample. Animals reaching Day 1 young adult stage prior to egg laying were used to analyze ventral nerve cord cell deaths. V9-V12 cells were visualized and quantified with the Plin-11p::GFP fluorescence reporter.

ER and osmotic stress treatments

For ER stress induction, TM (Tunicamycin T7765, Sigma-Aldrich) was dissolved in DMSO as a 5 mg/ml stock and diluted into a final concentration specified in each experiment on the OP50/NGM medium plate. For osmotic stress, NaCl (S7653, Sigma-Aldrich) was dissolved in MiliQ H_2O as a 4 M stock and diluted into a final concentration specified in each experiment on the OP50/NGM medium plate. 6ug/ml TM is used for Phsp-4::GFP induction in adult, 2ug/ml TM is used for Phsp-4::GFP induction in young larvae. 400 mM NaCl is used for Pnlp-

29::GFP induction in adult, 200 mM NaCl is used for Pnlp-29::GFP induction in young larvae.

Nomarski DIC and fluorescence imaging

Animals were imaged with a Zeiss Axioplan2 fluorescent microscope equipped with Nomarski DIC optics and a Hamamatsu ORCA C13440 camera. Zeiss Zen Imaging software v2.5 and v3.4 Pro were used for image collection. Same exposure time for all animals in each experiment. Fiji (1.54 f) was used for fluorescence quantification.

Western blots

Synchronous animals were collected in M9 and snap frozen with liquid nitrogen. Pellets were sonicated in lysis buffer containing 50 mM Tris, pH 8.0, 1 mM EDTA, 50 mM NaCl, 0.5% NP-40, 1x Halt Protease Inhibitor Cocktails (Fisher Scientific, PI78440) on ice. Approximately 12 µg of total protein (35 µg total protein for over-exposure experiment of *ced-3* promoter reporter without uTFs) was loaded per well and resolved on 4–20% gradient acrylamide gels. The *ced-3* promoter reporter generating the His-24::mCherry::AID::HA fusion protein was detected using anti-HA antibody. Anti-HA antibody from rabbit (Cell Signaling Technology, 3724S) was used at 1:1,500 dilution. For loading control, anti-actin (Bio-Rad, 12004163) antibody was used at 1:5,000 dilution. BioRad ChemiDoc MP Imaging system with image Lab Touch v.2.3.0.07 was used for Western Blot imaging and quantification.

Generation of biotinylated DNA probes

Primers with 5′-biotinylation were used to amplify the uTFs DNA element -2542bp to -1619bp upstream of *ced-3* gene with gDNA extracted from wild-type animals. As a control, +33 bp to +935 bp of mCherry coding sequence was amplified using 5′-biotinylated primers. See Supplementary Table 3 for oligos used for amplification. Amplified PCR product was purified and concentrated with Amicon Ultra centrifugal concentration unit (Sigma) at final concentration of 200 ng/µL.

Mass-spectrometric identification of proteins binding *ced-3* uTFs

Biotinylated DNA was incubated with Dynabeads (Thermofisher) at room temperature for 30 min with reaction buffer to form bead-DNA complex. Lysates of synchronized L3 larvae was incubated with probe bound beads for 60 minutes in the presence of 1x Halt Protease and phosphatase inhibitor cocktail (Thermofisher) at room temperature in the presence of 50 µg of salmon sperm DNA. After washing 5 times with reaction buffer containing 25 mM Tris pH7.5, 1 mM EDTA, 10% Sucrose, 15% Glycerol, 65 mM NaCl, 5 mM CaCl2, 50 mM KCl and 10 mM HEPES followed by 3 times wash with TE buffer pH7.5. Magnetic beads were sent for on bead trypsinization, desalting, mass-spectrometry analyses and protein ID performed by the UTSW proteomics core. Specifically, samples were digested overnight with trypsin (Pierce) following reduction and alkylation with DTT and iodoacetamide (Sigma–Aldrich). Following solid-phase extraction cleanup with an Oasis HLB µelution plate (Waters), the resulting peptides were reconstituted in 10 uL of 2% (v/v) acetonitrile (ACN) and 0.1% trifluoroacetic acid in water. 5 µL of each sample was injected onto an Orbitrap Fusion Lumos mass spectrometer coupled to an Ultimate 3000 RSLC-Nano liquid chromatography systems (Thermo). Samples were injected onto a 75 µm i.d., 75-cm long EasySpray column (Thermo), and eluted with a gradient from 0-28% buffer B over 90 min. Buffer A contained 2% (v/v) ACN and 0.1% formic acid in water, and Buffer B contained 80% (v/v) ACN, 10% (v/v) trifluoroethanol, and 0.1% formic acid in water. The mass spectrometer operated in positive ion mode with a source voltage of 2.0 kV and an ion transfer tube temperature of 300 °C. MS scans were acquired at 120,000 resolution in the Orbitrap and up to 10 MS/MS spectra were obtained in the Orbitrap for each full spectrum acquired using higher-energy collisional dissociation (HCD) for ions with charges 2-7. Dynamic exclusion was set for 25 s after an ion was selected for fragmentation.

Raw MS data files were analyzed using Proteome Discoverer v.2.4 SP1 (Thermo), with peptide identification performed using a trypsin digest search with Sequest HT (cleavage after Lys and Arg except when followed by Pro). The *C. elegans* reviewed protein database from UniProt (downloaded March 18, 2020, 26942 entries) was used. Fragment and precursor tolerances of 10 ppm and 0.6 Da were specified, and three missed cleavages were allowed. A minimum peptide length of 6 residues was required, and at least 2 unique peptides were required for positive protein identification. Carbamidomethylation of Cys was set as a fixed modification and oxidation of Met was set as a variable modification. The false-discovery rate (FDR) cutoff was 1% for all peptides and proteins. Proteins enriched for binding to uTFs versus control mCherry DNA probe were determined with the following criteria: FDR < 0.01, unique peptides ≥ 2, abundance fold change > 2. Proteins with DNA binding function were prioritized for further analyses.

RNAi screen of proteins binding *ced-3* uTFs promoter region

RNAi screen was performed on NGM plates supplemented with 200 µg/ml ampicillin and 1 mM IPTG and seeded with HT115 expressing RNAi construct. Synchronous early larval animals were first placed on plates for RNAi treatment until reaching early L4 larval stage. Then animals were treated with 3 µg/ml Tunicamycin or 350 mM NaCl in the presence of RNAi. The induction of P*hsp-4*::GFP or Pnlp-29::GFP were imaged and quantified 16 hours after stress treatment.

UV stress treatment and aging survival assay

For UV irradiation, similar number of synchronous animals placed on plates seeded with OP50 or RNAi were treated with indicated dose using XL1500 UV CROSSLINKER. For young larvae, synchronous L1 or L2 were irradiated with 4 mJ/cm^2 (L1 larvae) or 8 mJ/cm^2 (L2 larvae) energy. L1 larvae of *glp-4(bn2)* mutants were treated with 3 mJ/cm^2 UV energy. Developmental stages of UV irradiated or control animals were recorded 48 hours after treatment. The *xpd-1(ve842)* mutants were recorded 72 hours after treatment due to developmental delay. Comparisons were made to non-treated animals for alterations in developmental rate. For survival curve in adult, synchronized early L4 larvae (*xpd-1(ve842)* mutant) or mid-L4 (all other strains) were exposed to either 75 mJ/cm^2 (OP50 food) or 100 mJ/cm^2 (HT115 food) UV energy. Twenty animals from each genotype or RNAi treatment were randomly selected immediately after irradiation and transferred to a new plate for survival counting every 24 hours. Three replicates of each genotype were analyzed in each experiment and two independent experiments were performed to confirm the findings.

Germline and whole body degradation of CED-3

Animals expressing CED-3::AID tagged protein were crossed with either *eft-3* promoter or *sun-1* promoter driven TIR1 E3 ligase for whole body and germline specific elimination of CED-3, respectively. To eliminate CED-3, animals were fed OP50 combined with 0.5mM K-NAA (auxin analog) on NGM plates. Animals expressing CED-3::AID tagged protein without TIR1 E3 ligase were used as negative control.

HEK proliferation assay

HEK293 cells transfected with siRNA were plated on 24-well plates with No.1.5 polymer coverslip bottom (ibidi 82426). After overnight transfection with siRNA, cells were irradiated with 15 mJ/cm^2 energy. Label free cell counting was performed with Agilent Cytation C10 imager (Gen5 v3.15) coupled with BioSpa (v 1.04) at 5% CO2 and 37 °C humidified chamber. Images of the same coordinance in a given well were taken every 6 hours out to 48 hours. Growth curve was plotted using three biological replicates and fitted using logistic growth curve with maximum set to 25000 cells (Graphpad Prism 10).

Cyclobutane pyrimidine dimer (CPD) quantification

Synchronized L4 animals were treated with 75 mJ/cm^2 UV and allowed to recover for 16 hours before collecting for gDNA isolation using Monarch® Genomic DNA Purification Kit (NEB T3010S). CPD measurement was performed using OxiSelect™ UV-Induced DNA Damage ELISA Kit (Cell BioLabs INC, STA-322) following manufacturer protocol. In brief, 4 µg/mL gDNA were diluted 2-fold with Reduced DNA and bound to DNA high-binding plate overnight. After incubating 1 hour at room temperature with anti-CPD antibodies, wells were washed 5 times. Following 1 hour incubation with secondary antibody-HRP Conjugate, wells were washed again 5 times. Substrate was then added to each well and incubated for 1 minute before adding stop solution. Absorbance of each well were read at 450 nm wave length using Agilent BioTek plate reader (Gen5 V3.11).

Statistics and reproducibility

Statistical analyses, sample size, replication, p values and estimates of error are provided in figures and figure legends.

Reporting summary

Further information on research design is available in the Nature Portfolio Reporting Summary linked to this article.

Data availability

Data generated in this study are provided in the Source data file and Supplementary Dataset. Source data are provided with this paper.

References

1. Ellis, H. M. & Horvitz, H. R. Genetic control of programmed cell death in the nematode C. elegans. *Cell* **44**, 817–829 (1986).
2. Yuan, J. Y. & Horvitz, H. R. The Caenorhabditis elegans genes ced-3 and ced-4 act cell autonomously to cause programmed cell death. *Dev. Biol.* **138**, 33–41 (1990).
3. Yuan, J., Shaham, S., Ledoux, S., Ellis, H. M. & Horvitz, H. R. The C. elegans cell death gene ced-3 encodes a protein similar to mammalian interleukin-1 beta-converting enzyme. *Cell* **75**, 641–652 (1993).
4. Arama, E., Bader, M., Rieckhof, G. E. & Steller, H. A ubiquitin ligase complex regulates caspase activation during sperm differentiation in Drosophila. *PLoS Biol.* **5**, e251 (2007).
5. Dick, S. A. et al. Caspase 3 cleavage of Pax7 inhibits self-renewal of satellite cells. *Proc. Natl. Acad. Sci. USA* **112**, E5246–E5252, https://doi.org/1512869112 (2015).
6. Fujita, J. et al. Caspase activity mediates the differentiation of embryonic stem cells. *Cell Stem Cell* **2**, 595–601, https://doi.org/S1934-5909(08)00162-8 (2008).
7. Weaver, B. P., Weaver, Y. M., Mitani, S. & Han, M. Coupled caspase and N-end rule ligase activities allow recognition and degradation of pluripotency factor LIN-28 during non-apoptotic development. *Dev. Cell* **41**, 665–673, https://doi.org/S1534-5807(17)30395-7 (2017).
8. Mishra, N., Wei, H. & Conradt, B. Caenorhabditis elegans ced-3 caspase is required for asymmetric divisions that generate cells programmed to die. *Genetics* **210**, 983–998 (2018).
9. Pinan-Lucarre, B. et al. The core apoptotic executioner proteins CED-3 and CED-4 promote initiation of neuronal regeneration in Caenorhabditis elegans. *PLoS. Biol.* **10**, e1001331 (2012).
10. Campbell, D. S. & Okamoto, H. Local caspase activation interacts with Slit-Robo signaling to restrict axonal arborization. *J. Cell Biol.* **203**, 657–672 (2013).
11. Weghorst, F., Mirzakhanyan, Y., Hernandez, K. L., Gershon, P. D. & Cramer, K. S. Non-apoptotic caspase activity preferentially targets a novel consensus sequence associated with cytoskeletal proteins in the developing auditory brainstem. *Front Cell Dev. Biol.* **10**, 844844 (2022).
12. Geden, M. J., Romero, S. E. & Deshmukh, M. Apoptosis versus axon pruning: Molecular intersection of two distinct pathways for axon degeneration. *Neurosci. Res.* **139**, 3–8 (2019).
13. Judy, M. E. et al. A shift to organismal stress resistance in programmed cell death mutants. *PLoS. Genet* **9**, e1003714 (2013).
14. Weaver, B. P. et al. Non-canonical caspase activity antagonizes p38 MAPK stress-priming function to support development. *Dev. Cell* **53**, 358–369.e356 (2020).
15. Yuan, W. et al. Modulating p38 MAPK signaling by proteostasis mechanisms supports tissue integrity during growth and aging. *Nat. Commun.* **14**, 4543 (2023).
16. Xu, D. C., Wang, L., Yamada, K. M. & Baena-Lopez, L. A. Non-apoptotic activation of Drosophila caspase-2/9 modulates JNK signaling, the tumor microenvironment, and growth of wound-like tumors. *Cell Rep.* **39**, 110718 (2022).
17. Perez, E., Lindblad, J. L. & Bergmann, A. Tumor-promoting function of apoptotic caspases by an amplification loop involving ROS, macrophages and JNK in Drosophila. *Elife* **6**, https://doi.org/10.7554/eLife.26747 (2017).
18. Sullivan, G. P. et al. TRAIL receptors serve as stress-associated molecular patterns to promote ER-stress-induced inflammation. *Dev. Cell* **52**, 714–730.e715 (2020).
19. Brunette, S., Sharma, A., Bell, R., Puente, L. & Megeney, L. A. Caspase 3 exhibits a yeast metacaspase proteostasis function that protects mitochondria from toxic TDP43 aggregates. *Micro. Cell* **10**, 157–169 (2023).
20. Burguillos, M. A. et al. Caspase signalling controls microglia activation and neurotoxicity. *Nature* **472**, 319–324 (2011).
21. Diot, C. et al. Bacterial diet modulates tamoxifen-induced death via host fatty acid metabolism. *Nat. Commun.* **13**, 5595 (2022).
22. Wei, H. et al. Proteolytic activation of fatty acid synthase signals pan-stress resolution. *Nat. Metab.* https://doi.org/10.1038/s42255-023-00939-z (2024).
23. Wilson, C. H. et al. Age-related proteostasis and metabolic alterations in Caspase-2-deficient mice. *Cell Death. Dis.* **6**, e1615 https://doi.org/cddis2014567 (2015).
24. Shalini, S. et al. Caspase-2 protects against oxidative stress in vivo. *Oncogene* **34**, 4995–5002, https://doi.org/onc2014413 (2015).
25. Ando, K. et al. NPM1 directs PIDDosome-dependent caspase-2 activation in the nucleolus. *J. Cell Biol.* **216**, 1795–1810 (2017).
26. Kim, J. Y. et al. ER stress drives lipogenesis and steatohepatitis via caspase-2 activation of S1P. *Cell* **175**, 133–145 e115 (2018).
27. Zhou, Z., Hartwieg, E. & Horvitz, H. R. CED-1 is a transmembrane receptor that mediates cell corpse engulfment in C. elegans. *Cell* **104**, 43–56 (2001).
28. Shaham, S., Reddien, P. W., Davies, B. & Horvitz, H. R. Mutational analysis of the Caenorhabditis elegans cell-death gene ced-3. *Genetics* **153**, 1655–1671 (1999).
29. Zhang, L., Hammell, M., Kudlow, B. A., Ambros, V. & Han, M. Systematic analysis of dynamic miRNA-target interactions during C. elegans development. *Development* **136**, 3043–3055 (2009).
30. Au, V. et al. CRISPR/Cas9 methodology for the generation of knockout deletions in Caenorhabditis elegans. *G3 (Bethesda)* **9**, 135–144 (2019).
31. Reddien, P. W., Andersen, E. C., Huang, M. C. & Horvitz, H. R. DPL-1 DP, LIN-35 Rb and EFL-1 E2F act with the MCD-1 zinc-finger protein to promote programmed cell death in Caenorhabditis elegans. *Genetics* **175**, 1719–1733 (2007).
32. Stergiou, L., Eberhard, R., Doukoumetzidis, K. & Hengartner, M. O. NER and HR pathways act sequentially to promote UV-C-induced germ cell apoptosis in Caenorhabditis elegans. *Cell Death Differ.* **18**, 897–906 (2011).
33. Wang, S., Meyer, D. H. & Schumacher, B. Inheritance of paternal DNA damage by histone-mediated repair restriction. *Nature* **613**, 365–374 (2023).

34. Volkova, N. V. et al. Mutational signatures are jointly shaped by DNA damage and repair. *Nat. Commun.* **11**, 2169 (2020).
35. Ito, S. et al. MMXD, a TFIIH-independent XPD-MMS19 protein complex involved in chromosome segregation. *Mol. Cell* **39**, 632–640 (2010).
36. Liu, H. et al. Structure of the DNA repair helicase XPD. *Cell* **133**, 801–812 (2008).
37. Greber, B. J., Toso, D. B., Fang, J. & Nogales, E. The complete structure of the human TFIIH core complex. *Elife* **8** https://doi.org/10.7554/eLife.44771 (2019).
38. Peissert, S. et al. In TFIIH the Arch domain of XPD is mechanistically essential for transcription and DNA repair. *Nat. Commun.* **11**, 1667 (2020).
39. Lehmann, A. R. The xeroderma pigmentosum group D (XPD) gene: one gene, two functions, three diseases. *Genes Dev.* **15**, 15–23 (2001).
40. Taylor, E. M. et al. Xeroderma pigmentosum and trichothiodystrophy are associated with different mutations in the XPD (ERCC2) repair/transcription gene. *Proc. Natl. Acad. Sci. USA* **94**, 8658–8663 (1997).
41. Wang, X. W. et al. The XPB and XPD DNA helicases are components of the p53-mediated apoptosis pathway. *Genes Dev.* **10**, 1219–1232 (1996).
42. Rieckher, M. et al. Distinct DNA repair mechanisms prevent formaldehyde toxicity during development, reproduction and aging. *Nucleic Acids Res.* **52**, 8271–8285 (2024).
43. Lans, H. et al. Involvement of global genome repair, transcription coupled repair, and chromatin remodeling in UV DNA damage response changes during development. *PLoS Genet* **6**, e1000941 (2010).
44. Thijssen, K. L. et al. C. elegans TFIIH subunit GTF-2H5/TTDA is a non-essential transcription factor indispensable for DNA repair. *Commun. Biol.* **4**, 1336 (2021).
45. Compe, E. & Egly, J. M. TFIIH: when transcription met DNA repair. *Nat. Rev. Mol. Cell Biol.* **13**, 343–354 (2012).
46. Cao, K. et al. Mitochondrial dynamics regulate genome stability via control of caspase-dependent DNA damage. *Dev. Cell* **57**, 1211–1225 e1216 (2022).
47. Rao, R. V. et al. Coupling endoplasmic reticulum stress to the cell death program. Mechanism of caspase activation. *J. Biol. Chem.* **276**, 33869–33874 (2001).
48. Katoh, I., Tomimori, Y., Ikawa, Y. & Kurata, S. Dimerization and processing of procaspase-9 by redox stress in mitochondria. *J. Biol. Chem.* **279**, 15515–15523 (2004).
49. Lamkanfi, M. et al. Targeted peptidecentric proteomics reveals caspase-7 as a substrate of the caspase-1 inflammasomes. *Mol. Cell Proteom.* **7**, 2350–2363 (2008).
50. Zuo, Y. et al. Oxidative modification of caspase-9 facilitates its activation via disulfide-mediated interaction with Apaf-1. *Cell Res.* **19**, 449–457 (2009).
51. Ross, C. et al. Inflammatory caspases: toward a unified model for caspase activation by inflammasomes. *Annu. Rev. Immunol.* **40**, 249–269 (2022).
52. Amcheslavsky, A. et al. Plasma membrane localization of apoptotic caspases for non-apoptotic functions. *Dev. Cell* **45**, 450–464 e453 (2018).
53. Hipp, M. S., Kasturi, P. & Hartl, F. U. The proteostasis network and its decline in ageing. *Nat. Rev. Mol. Cell Biol.* **20**, 421–435 (2019).
54. Labbadia, J. & Morimoto, R. I. The biology of proteostasis in aging and disease. *Annu. Rev. Biochem* **84**, 435–464 (2015).
55. Arantes-Oliveira, N., Apfeld, J., Dillin, A. & Kenyon, C. Regulation of life-span by germ-line stem cells in Caenorhabditis elegans. *Science* **295**, 502–505 (2002).
56. Ermolaeva, M. A. et al. DNA damage in germ cells induces an innate immune response that triggers systemic stress resistance. *Nature* **501**, 416–420 (2013).
57. Soltanmohammadi, N., Wang, S. & Schumacher, B. Somatic PMK-1/p38 signaling links environmental stress to germ cell apoptosis and heritable euploidy. *Nat. Commun.* **13**, 701 (2022).
58. Bujarrabal-Dueso, A. et al. The DREAM complex functions as conserved master regulator of somatic DNA-repair capacities. *Nat. Struct. Mol. Biol.* **30**, 475–488 (2023).

Acknowledgements

We thank the CGC (funded by NIH Office of Research Infrastructure Programs [P40 OD010440]) for materials; WormBase, The Alliance of Genome Resources, The Gene Ontology Knowledgebase, and UniProt database. Protein mass-spectrometry was performed and analyzed by the UT Southwestern Proteomics Core facility. This work is supported by Welch Foundation grant I-2022-20190330 (B.P.W.) and National Institutes of Health grants R35GM133755 (B.P.W.) and R21AG086710 (B.P.W.). The content is solely the responsibility of the authors and does not necessarily represent the official views of the funding bodies.

Author contributions

H.W., Y.M.W., and B.P.W. conceived the study and designed research; H.W., Y.M.W. performed research; H.W., Y.M.W., and B.P.W. analyzed data; H.W., Y.M.W., and B.P.W. wrote the manuscript; Y.M.W. and B.P.W. supervised the study; B.P.W. acquired funding.

Competing interests

The authors declare no competing interests.

Additional information

Supplementary information The online version contains supplementary material available at https://doi.org/10.1038/s41467-024-53755-8.

Correspondence and requests for materials should be addressed to Benjamin P. Weaver.

Peer review information *Nature Communications* thanks the anonymous reviewers for their contribution to the peer review of this work. A peer review file is available.